J. Biophotonics **9**, No. 10, 987–993 (2016) / **DOI** 10.1002/jbio.201600125

Journal of BIOPHOTONICS

LETTER

Biodistribution of inhaled metal oxide nanoparticles mimicking occupational exposure: a preliminary investigation using enhanced darkfield microscopy

Marissa Guttenberg[**,1], *Leonardo Bezerra*[**,1], *Nicole M. Neu-Baker*[1], *María del Pilar Sosa Idelchik*[1], *Alison Elder*[2], *Günter Oberdörster*[2], *and Sara A. Brenner*[*,1]

[1] State University of New York (SUNY) Polytechnic Institute, College of Nanoscale Science, Nanobioscience Constellation, 257 Fuller Road, Albany, New York, 12203, United States
[2] University of Rochester, Department of Environmental Medicine, 601 Elmwood Avenue, Rochester, New York, 14642, United States

Received 27 April 2016, revised 24 June 2016, accepted 25 July 2016
Published online 16 August 2016

Key words: inhalation exposure, enhanced darkfield microscopy, engineered nanomaterials, histological samples

Inhalation exposure to engineered nanomaterials (ENMs) may result in adverse pulmonary and/or systemic health effects. In this study, enhanced darkfield microscopy (EDFM) was used as a novel approach to visualizing industrial metal oxide nanoparticles (NPs) (silica, ceria, or alumina) in multiple tissue types following inhalation in rats mimicking occupational exposures. Advantages of EDFM over electron microscopy (EM) include reduced cost, time, and ease of sample preparation and operation. Following 4–6 hour inhalation exposures at three concentrations (3.5–34.0 mg/m^3), lungs and secondary organs were harvested at 24 hours or 7 days post-exposure and prepared for brightfield (BF) microscopy and EDFM. NPs were visualized within the lung and associated lymphatic tissues and in major organs of excretion (liver, spleen, kidney). EDFM also revealed NPs within pulmonary blood vessels and localization within specific regions of toxicological relevance in liver and kidney, indicating pathways of excretion. Results demonstrate the utility of EDFM for rapid direct visualization of NPs in various tissue types and suggest the potential for metal oxide NPs to distribute to secondary tissues following inhalation exposure. Confirmation of the composition, distribution, and relative abundance of inhaled NPs will be pursued by combining EDFM with hyperspectral imaging (HSI) and mapping.

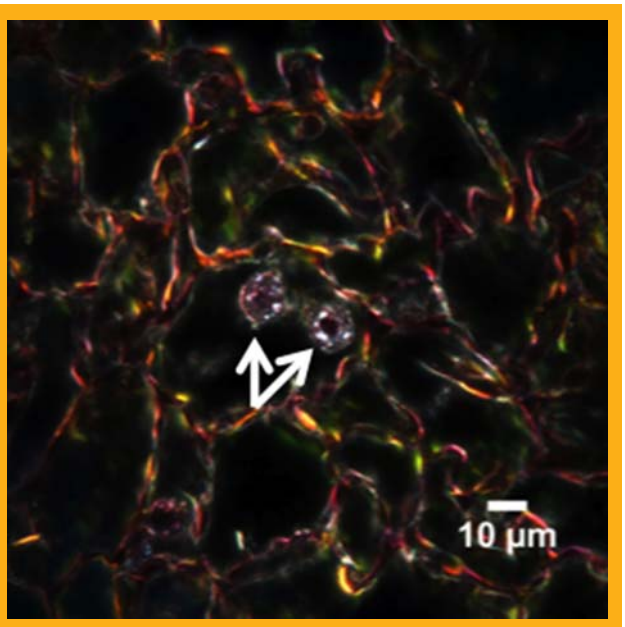

* Corresponding author: e-mail: sbrenner@sunypoly.edu
** These authors contributed equally to this work.

Journal of BIOPHOTONICS

1. Introduction

Engineered nanomaterials (ENMs) are increasingly incorporated into a variety of consumer products. An ENM is an intentionally manufactured material with at least one external dimension in the size range from approximately 1–100 nanometers (nm). The Project on Emerging Nanotechnologies has been tracking nano-enabled consumer products and currently lists 1,814 consumer products containing ENMs from 622 companies in 32 countries, up from 54 products when the inventory was launched in 2005 [1]. In addition to consumer products, ENMs are also being incorporated into manufacturing processes in a variety of industries [2, 3] and into pharmaceuticals for enhanced efficacy and improved drug delivery [4, 5]. As the production and use of ENMs increases, the potential for exposure (intentional and unintentional) and related biological effects also increases for workers, patients, and the general public.

A common challenge shared by toxicology and biomedical researchers is the ability to rapidly visualize and identify nanomaterials (NMs) in cells and tissues [6, 7]. The current best-known method for direct visualization of NMs is electron microscopy (EM), often coupled with energy dispersive X-ray spectroscopy (EDS) for elemental identification [8]. However, rapid identification and characterization of NMs in biological samples and other forms of complex media, such as environmental media, is hindered by the associated cost and time required to perform EM [9, 10]. This analytical bottleneck is slowing progress in many disciplines where nanoscale visualization and characterization are critical. Enhanced darkfield microscopy (EDFM) offers a more rapid and less costly alternative to EM for direct visualization of NMs in complex matrices [9, 10]. The CytoViva enhanced darkfield microscope has a patented condenser that improves alignment and focus of oblique angle illumination, thereby enhancing the signal-to-noise up to seven times over standard darkfield optics and allowing for improved visualization of nanoscale materials. Coupled with hyperspectral imaging (HSI), EDFM provides a method for visualization and nanoparticle (NP) identification based on hyperspectral data. While EM is capable of higher magnification and resolution than EDFM-HSI, there is also considerable time-to-knowledge, cost-of-ownership ($ 1–4M for transmission EM vs. $ 155,000 for EDFM-HSI), and intensive training for tool operation that is not the case with EDFM [10]. For example, rapid scanning of a 1.5 cm × 1.5 cm tissue sample with EDFM at 10–100× magnification takes a trained microscopist less than 1 hr, while it would take a minimum of 5 months (8 hr/day, 5 days/week) to scan the same sample area with transmission EM at "low" 1,000× magnification [10]. Further, samples for EDFM need only be prepared as for light microscopy, which is commonly performed at most histology cores; special handling and preparation, including stains, fluorescent markers or creation of thin sections for EM, are not required. As such, EDFM is an attractive alternative method for rapid scanning of samples containing NPs.

This study investigated the application of EDFM to identify NMs *in situ* in tissue samples obtained from rats sacrificed post-inhalation exposure to metal oxide nanoparticles (NPs) currently used in industrial settings. The goal of this preliminary investigation was to identify and characterize the retention and location of NPs in the lungs (alveolar space, blood vessels, macrophages), assess the potential for NP biodistribution to other organs, and identify specific locations of NPs within anatomical regions of each organ using EDFM.

2. Experimental

In this study, male F344 rats (8–10 weeks old; n = 16) were exposed for 4–6 hours via inhalation to aerosolized metal oxide NPs in aqueous suspensions at 3 concentrations ranging between 3.5 mg/m^3 and 34.0 mg/m^3 (as the NPs; see Table 1). Animal protocols were approved by the Institutional Animal Care and Use Committee (IACUC) at the University of Rochester. The NP suspensions were comprised of synthetic amorphous silica (SiO_2), alumina (Al_2O_3), or ceria (CeO_2) NPs with dispersants, surfactants, and acids or bases in deionized water. Controls were exposed to filtered air. The primary NP sizes were characterized by scanning electron microscopy (SEM) with EDS (Table 1; Supporting Information [11]). The agglomerate sizes in the slurry-containing aerosols were evaluated using a cascade impactor and are reported here as mass median aerodynamic diameters (MMAD) with geometric standard deviations (GSD): for silica: MMAD, 0.6–0.8 μm; GSD, 1.8; for alumina: MMAD, 1.0–1.6 μm; GSD, 1.6–1.7; for ceria: MMAD, 0.8–1.0 μm; GSD, 1.5–1.6. These data show that the individual NPs were organized into ~1 μm agglomerates when they were inhaled.

Rats were sacrificed at different time points, either 24 hours or 7 days post-exposure, and organs (lungs, lung lymph nodes, liver, kidney and spleen) were harvested. Following exposure, tissues (other than lung) were fixed via immersion in 4% paraformaldehyde for 24 hr, then transferred to phosphate buffered saline (PBS) and stored in PBS until histological preparation by the Albany Medical College Histology Core (Albany, NY). Lungs were fixed via the trachea at a hydrostatic pressure of 30 cm H_2O to maintain tissue architecture. Fixed tissues were bi-

Table 1 Nanoparticle concentrations for inhalation exposure.

Slurry Type	Primary Particle Sizes (nm) by SEM* [11][a]	Level of Exposure	Nanoparticle Concentration (mg/m^3)[b]
Silica	29.7 ± 6.8	Low	4.6
		Medium	16.3
		High	34.0
Alumina	20.3[c] ± 4.3	Low	9.7
		Medium	18.1
		High	20.9
Ceria	35.0 ± 15.4	Low	3.5
		Medium	7.4
		High	9.5

* The particles were sized as previously described (see Supporting Information and Roth et al. 2015b for more detail) [11]. Note that these particle size ranges do not reflect the aerosol size distributions to which the rats were exposed.
[a] Values are means ± SD.
[b] These values are calculated from the means of the daily total mass concentrations and the measured amount of SiO_2, Al_2O_3, and CeO_2, respectively, in each slurry.
[c] Appeared as "N/A" in Roth et al. Diameter of 20.3 nm was obtained after refinement of imaging techniques.

sected, processed through solvents, and embedded in paraffin using a Leica Tissue Processor (Leica; Wetzlar, Germany). Paraffin-embedded tissues were sectioned (6 μm thickness) using a rotary microtome with a clean blade for each cut to minimize cross-contamination and mounted onto glass microscopy slides. Deparaffinized and rehydrated tissue sections were stained with hematoxylin and eosin (H&E), then dehydrated through graded alcohols to xylene and coverslipped [9, 10, 12, 13]. Tissue slides were scanned and imaged using BF microscopy, using a Nikon E200 brightfield microscope, and EDFM, using a CytoViva EDFM-HSI system (Auburn, AL) [9, 10]. Briefly, each slide was scanned in EDFM, where NPs are evident as bright spots or structures, and images were captured of NP-containing areas in EDFM, followed by BF for comparison and morphological analysis [9, 10].

3. Results and discussion

Resulting EDFM images allowed direct visualization of all three metal oxide NPs in all tissue types investigated. The visualization and localization of NPs appeared as high contrast structures seen by EDFM, while NPs in corresponding tissues samples imaged with BF were not readily visible. The negative control samples (exposed to filtered air) were imaged first with both modalities to assess the structure of tissue and organs, as shown in Figure 1. As expected, the 'normal' sample images show no indication of metallic luminescence in Figure 1, as compared to the following Figures. Figures 2–4 show BF and EDFM images of lung, lung lymph node (LLN), liver, kidney, and spleen tissues harvested from rats that were exposed via inhalation to silica, alumina, and ceria NPs, respectively at low, medium, or high concentrations for either 4 or 6 hours. Also, included in the supporting information, Figure S2 shows metal oxide NPs by EDFM in three different areas of physiological relevance in lung tissue: within the alveolar space, within the lumen of a blood vessel, and within lung macrophages. Of note, the samples investigated in this study were selected randomly from a much larger sample set containing multiple exposure groups designed for related inhalation toxicology research. Evident NPs illuminated as high-contrast structures in the EDFM images, whereas NPs appeared only as dark or black dots (if at all) in BF, and thus were not readily visible, as shown in all figures. The identification of NPs based on visualization with EDFM alone can be further characterized by HSI and mapping, as previously demonstrated by Sosa Peña et al. [10]. While BF was not an efficient modality for initial NP visualization, it proved to be valuable for assessing tissue architecture and morphology in samples from exposed animals, such as signs of inflammation in the liver characterized by dilated and congested vascular lumen [14], as seen in Figure 4.

The immediate next step in this investigation is to couple EDFM with HSI to confirm the composition of the NPs visualized by EDFM and to assess relative abundance and biodistribution via hyperspectral mapping. HSI, which is an emerging tool for the analysis of nanoscale materials in a variety of matrices, measures the intrinsic light scattering properties of object materials without the need for labeling or special sample preparation beyond what is necessary for light microscopy [15, 16]. Therefore, it holds promise not only for rapid optical and spectroscopic identification of NPs and NP agglomerates,

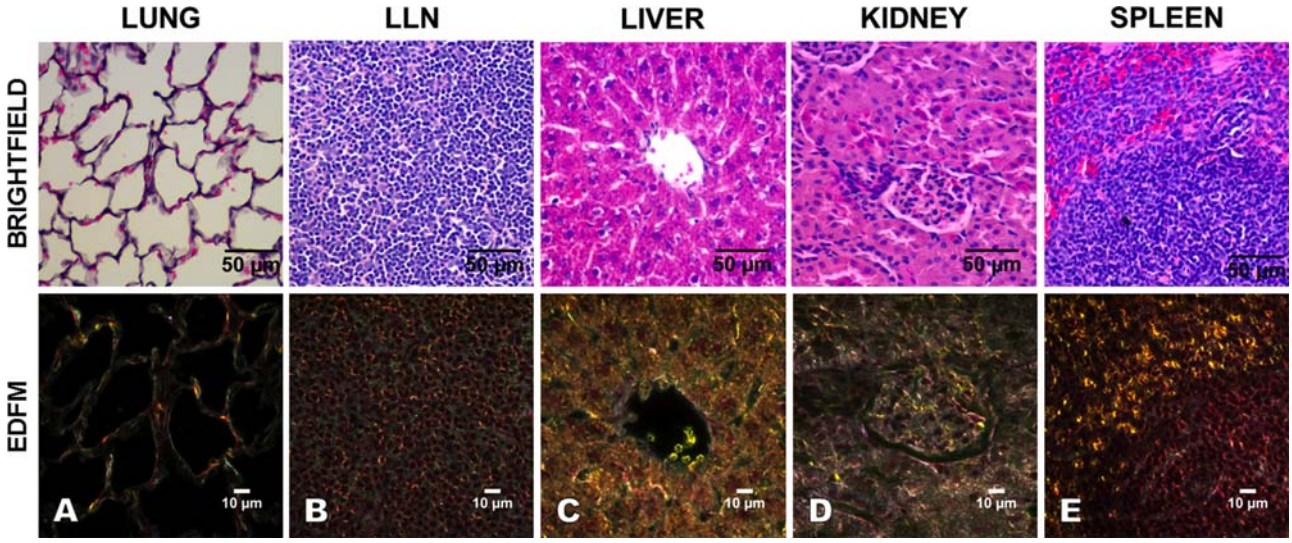

Figure 1 Negative control tissues imaged with brightfield (BF) and enhanced darkfield microscopy (EDFM). Negative control rats were exposed to filtered air for 6 hours and tissues were harvested at 24 hours post-exposure. Both BF (top row) and their respective EDFM images (bottom row) demonstrate the absence of high contrast elements or foreign NPs in these tissues and no signs of inflammation or physiological abnormalities. LLN, lung lymph node.

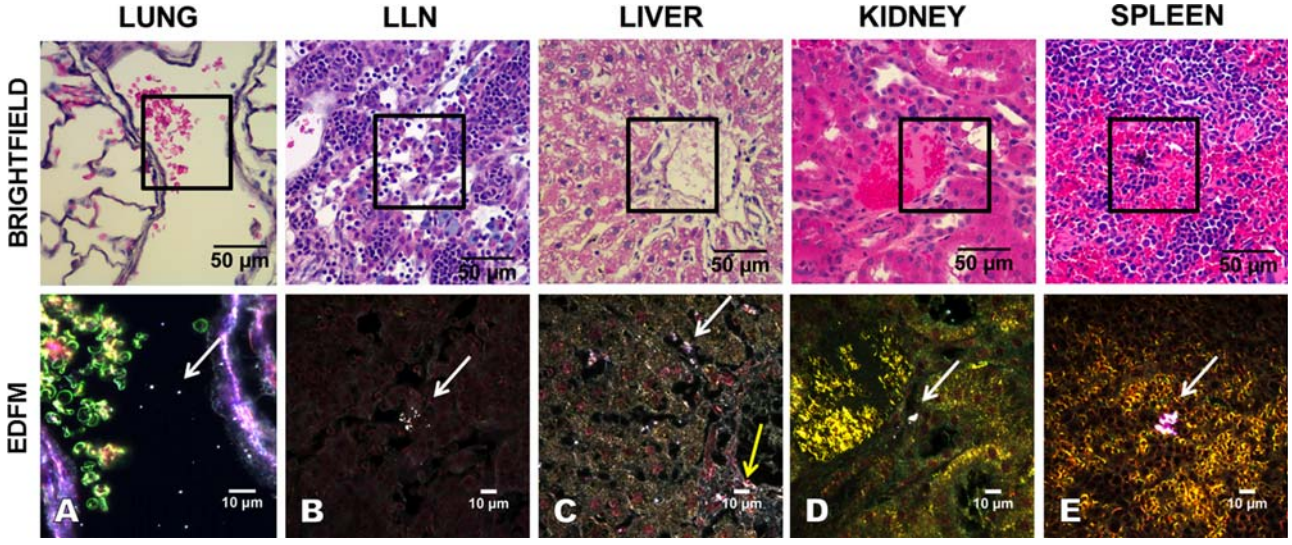

Figure 2 Biodistribution of nanoparticles (NPs) in organs of rats exposed via inhalation to silica NPs. The top row shows BF images taken at 40× magnification, with their respective EDFM images at 100× magnification shown in the bottom row. From left to right: (**A**) A blood vessel in the alveolar tissue of the lung contains multiple NPs (arrow) surrounded by red blood cells within the luminal space. This rat was exposed to a medium concentration (16.3 mg/m^3) of silica NP-containing slurry aerosol for 4 hours and sacrificed at 7 days post-exposure. (**B**) An agglomeration of NPs (arrow) is seen among multiple white blood cells in the lymph node. This rat was exposed to a high concentration (34.0 mg/m^3) of silica slurry aerosol for 4 hours and sacrificed at 24 hours post-exposure. (**C**) A portal triad in the liver with multiple NPs seen in both the connective tissue (yellow arrow) that supports its blood vessels and bile duct, and within the hepatic sinusoids (white arrow). This rat was exposed to a medium concentration (16.3 mg/m^3) of silica slurry aerosol for 4 hours and sacrificed at 24 hours post-exposure. (**D**) A cluster of NPs (arrow) is seen in the kidney among renal tubules and adjacent to a blood vessel in the renal cortex. This rat was exposed to a high concentration (34.0 mg/m^3) of silica slurry aerosol for 4 hours and sacrificed at 24 hours post-exposure. (**E**) Multiple agglomerated NPs (arrow) seen in the red pulp of the spleen. This rat was exposed to a high concentration (34.0 mg/m^3) of silica slurry aerosol for 4 hours and sacrificed at 7 days post-exposure.

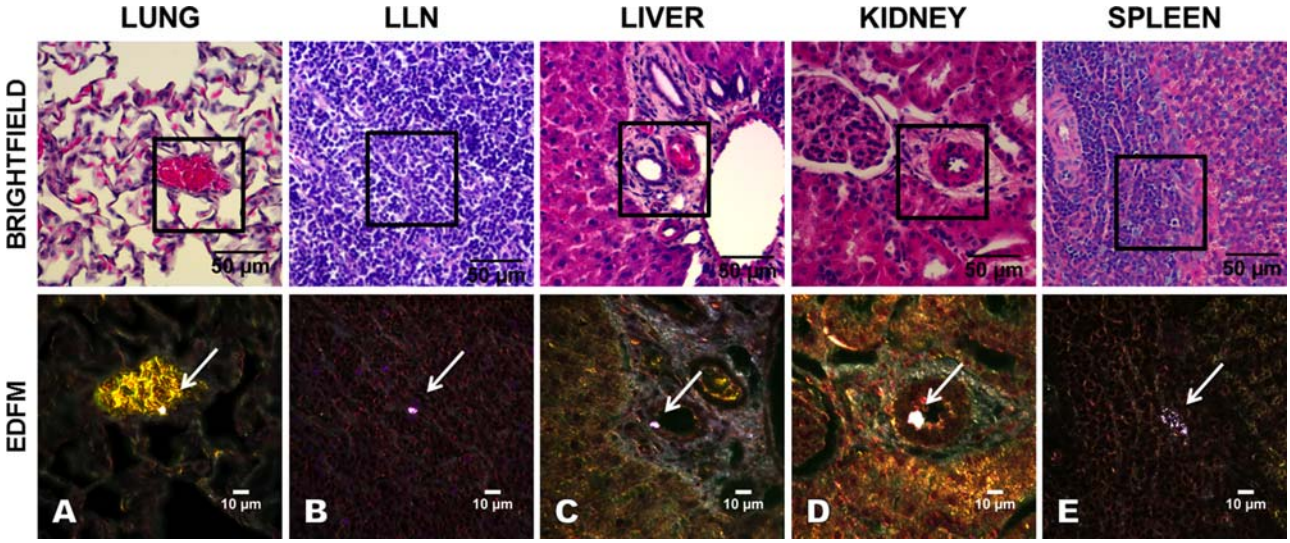

Figure 3 Biodistribution of NPs in organs of rats exposed via inhalation to alumina NPs. The top row shows BF images taken at 40× magnification, with their respective EDFM images at 100× magnification shown in the bottom row. From left to right: (**A**) A blood vessel (shown as a cross-section filled with red blood cells) in the alveolar tissue of the lung shows a cluster of NPs (arrow) located inside the vessel lumen surrounded by red blood cells that appear pink in BF and yellow in DF. This rat was exposed to a low concentration (9.7 mg/m^3) of alumina NP-containing slurry aerosol for 4 hours, and sacrificed at 7 days post-exposure. (**B**) A cluster of NPs (arrow) seen in a lung lymph node, surrounded by numerous white blood cells. This rat was exposed to a high concentration (20.9 mg/m^3) of alumina slurry for 6 hours, and sacrificed at 7 days post-exposure. (**C**) A cluster of NPs (arrow) seen in the epithelial cells lining the bile duct of a portal triad in the liver. This rat was exposed to a high concentration (20.9 mg/m^3) of alumina slurry aerosol for 6 hours, and sacrificed at 24 hours post-exposure. (**D**) A cluster of NPs (arrow) is seen in the endothelium lining a blood vessel in the kidney, adjacent to a glomerulus in the renal cortex. This rat was exposed to a low concentration (9.7 mg/m^3) of alumina slurry aerosol for 4 hours, and sacrificed at 24 hours post-exposure. (**E**) Multiple NPs (arrow) are shown agglomerated in the white pulp of the spleen. This rat was exposed to a high concentration (20.9 mg/m^3) of alumina slurry aerosol for 6 hours, and sacrificed at 7 days post-exposure.

but also as a screening tool for detecting the presence of ENMs in samples that could then be marked for further, more intensive analysis, for example, by EM. In order to assess NP composition and biodistribution in tissue, the research team will acquire hyperspectral images (datacubes) and map these images with reference spectral libraries (RSLs). The strengths and limitations of EDFM-HSI have been described [9, 10] and compared to those of EM, along with an assessment of accuracy, precision, reliability, efficiency, resource-intensity, and other technical and practical considerations for the use of EDFM-HSI in the analysis of samples containing NPs. Successful application of EDFM-HSI to the sample sets from this study could give way to a paradigm-shifting protocol that allows for rapid, cost-effective identification, relative quantitation, histological localization, and characterization for NPs in complex biological and environmental matrices.

4. Conclusion

The results of this preliminary investigation demonstrate the following key findings: 1) EDFM can be used to visually identify ENMs in a variety of tissue types, including localization within anatomical regions of interest; thus, EDFM provides a rapid, cost-effective alternative to conventional methods for direct visualization of ENMs in biological samples (due to faster, less expensive, and more readily available sample preparation and relative ease of training at the tool) and/or serve as a screening tool to identify a subset of samples for further analysis; 2) EDFM can be used in tandem with other methods (e.g., immunohistochemistry, standard histology/histopathology, EM, ICP-MS) by serial sectioning of the sample to provide complementary information; and 3) metal oxide NPs used in industrial settings, when inhaled, have the potential to translocate from deposits in the lung to different organs via the circulatory and lymphatic systems following inhalation exposure, similar to what has been shown for other poorly soluble NPs, and induce dose-dependent inflammatory responses.

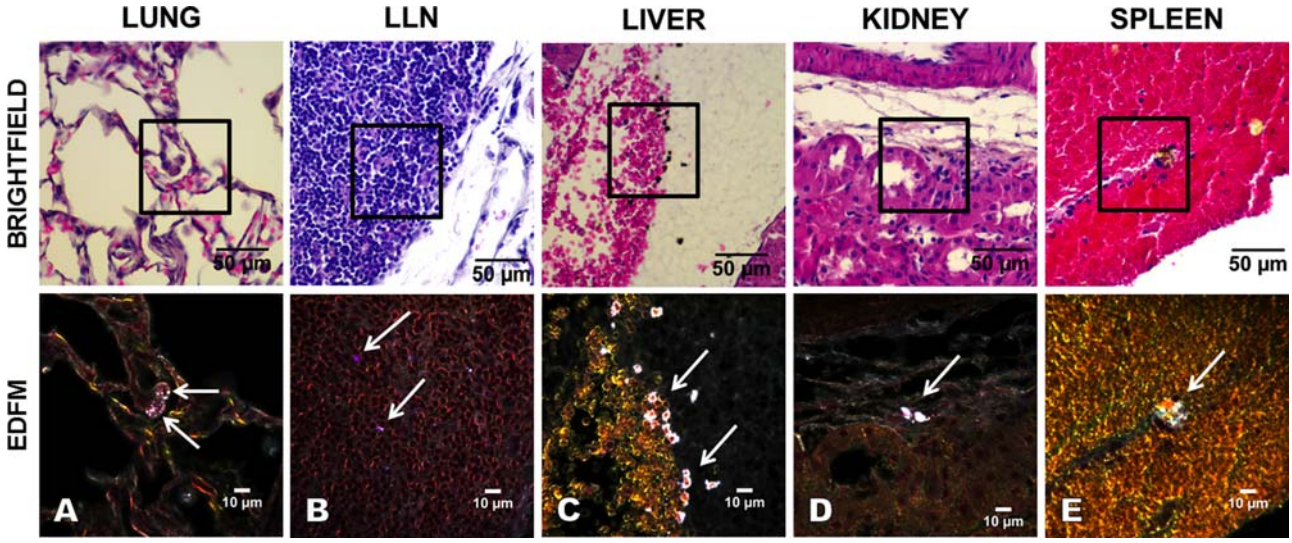

Figure 4 Biodistribution of NPs in organs of rats exposed via inhalation to ceria NPs. The top row shows BF images taken at 40× magnification, with their respective EDFM images at 100× magnification shown in the bottom row. From left to right, (**A**) Multiple NPs (arrows) are seen within two alveolar macrophages in the alveolar space of the lung. This rat was exposed to a medium concentration (7.4 mg/m^3) of ceria NP-containing slurry aerosol for 4 hours, and sacrificed at 7 days post-exposure. (**B**) Multiple NPs (arrows) are seen among the white blood cells in the lymph node. This rat was exposed to a high concentration (9.5 mg/m^3) of ceria slurry aerosol for 6 hours, and sacrificed at 24 hours post-exposure. (**C**) A central vein in the liver shows a dilated lumen congested with red blood cells and multiple NPs (arrows). This rat was exposed to a medium concentration (7.4 mg/m^3) of ceria slurry aerosol for 4 hours, and sacrificed at 7 days post-exposure. (**D**) Two clusters of NPs (arrow) are seen over the connective tissue adjacent to several tubules in the renal cortex. This rat was exposed to a high concentration (9.5 mg/m^3) of ceria slurry aerosol for 6 hours, and sacrificed at 24 hours post-exposure. (**E**) Multiple agglomerated NPs (arrow) are shown in the red pulp of the spleen surrounded by numerous red blood cells. This rat was exposed to a low concentration (3.5 mg/m^3) of ceria slurry aerosol for 4 hours, and sacrificed at 24 hours post-exposure.

Supporting Information

Additional supporting information may be found in the online version of this article at the publisher's website.

Acknowledgements The authors would like to acknowledge Julia Martinez and Zain-ul Sulehri for their contributions to microscopy and imaging the tissues presented here. Additionally, the authors thank Christina Rotondi (Albany Medical College Histology Core) for sample preparation and James Dillon for SEM and DLS work. This work was supported by CDC-NIOSH grant OH-009990-01A1 awarded to S.B.; NIEHS Center P30 grant ES01247 to A.E. and G.O.; and the NanoHealth and Safety Center, New York State, awarded to A.E., G.O., and S.B.

Author Contributions The manuscript was written through contributions of all authors. All authors have given approval to the final version of the manuscript.

Conflict of Interest Disclosure The authors declare no competing financial interest.

Abbreviations BF, brightfield; EDFM, enhanced dark-field microscopy; EDS, energy dispersive X-ray spectroscopy; EM, electron microscopy; ENM, engineered nanomaterial; H&E, hematoxylin & eosin; HSI, hyperspectral imaging; LLN, lung lymph node; NP, nanoparticle; PBS, phosphate buffered saline; RSL, reference spectral library.

References

[1] M. E. Vance, T. Kuiken, E. P. Vejerano, S. P. McGinnis, M. F. Hochella, Jr., D. Rejeski, and M. S. Hull, Beilstein J. Nanotechnol. **6**, 1769–1780 (2015).
[2] W. J. Stark, P. R. Stoessel, W. Wohlleben, and A. Hafner, Chem. Soc. Rev. **44**, 5793–5805 (2015).
[3] D. Speed, P. Westerhoff, R. Sierra-Alvarez, R. Draper, P. Pantano, S. Aravamudhan, K. L. Chen, K. Hristovski, P. Herckes, X. Bi, Y. Yang, C. Zeng, L. Otero-Gonzalez, C. Mikoryak, B. A. Wilson, K. Kosaraju, M. Tarannum, S. Crawford, P. Yi, X. Liu, S. V. Babu, M. Moinpour, J. Ranville, M. Montano, C. Corredor, J. Posner, and F. Shadman, Environ. Sci. **2**, 227–244 (2015).
[4] Q. Feng, J. Sun, and X. Jiang, Nanoscale (2016).
[5] X. Zhang, Cell Biochem. Biophys. **72**, 771–775 (2015).
[6] K.-H. Chen, D. J. Lundy, E. K.-W. Toh, C.-H. Chen, C. Shih, P. Chen, H.-C. Chang, J. J. Lai, P. S. Stayton, A. S. Hoffman, and P. C.-H. Hsieh, Nanoscale **7**, 15863–15872 (2015).

[7] J. Fujihara, M. Tongu, H. Hashimoto, T. Yamada, K. Kimura-Kataoka, T. Yasuda, Y. Fujita, and H. Takeshita, J. Med. Investig. **62**, 45–50 (2015).
[8] G. A. Roth, S. Tahiliani, N. M. Neu-Baker, and S. A. Brenner, Wiley Interdiscip. Rev. Nanomed. Nanobiotechnol. **7**, 565–579 (2015).
[9] G. A. Roth, M. P. Sosa Peña, N. M. Neu-Baker, S. Tahiliani, and S. A. Brenner, J. Vis. Exp. **106**, e53317 (2015a).
[10] M. P. Sosa Peña, A. Gottipati, S. Tahiliani, N. M. Neu-Baker, M. D. Frame, A. J. Friedman, and S. A. Brenner, Microsc. Res. Tech. **79**(5), 349–358 (2016).
[11] G. A. Roth, N. M. Neu-Baker, and S. A. Brenner, J. Chem. Heal. Saf. **22**, 26–32 (2015b).
[12] G. Kumar and J. Kiernan (Eds.), Special Stains and H&E (Dako North America, 2010).
[13] M. Titford, J. Histotechnol. **32**, 9–19 (2009).
[14] S. Alarifi, D. Ali, A. A. Al-Doaiss, B. A. Ali, and A. A. Al-Khedhairy, Int. J. Nanomedicine **8**, 3937–3943 (2013).
[15] A. R. Badireddy, M. R. Wiesner, and J. Liu, Environ. Sci. Technol. **46**, 10081–10088 (2012).
[16] J. N. Meyer, C. A. Lord, X. Y. Yang, E. A. Turner, A. R. Badireddy, S. M. Marinakos, A. Chilkoti, M. R. Wiesner, and M. Auffan, Aquat. Toxicol. **100**, 140–150 (2010).